JOURNAL OF APPLIED PHYSICS **117**, 115705 (2015)

Effect of the barrier growth mode on the luminescence and conductivity micron scale uniformity of InGaN light emitting diodes

M. J. Wallace,[1] P. R. Edwards,[1] M. J. Kappers,[2] M. A. Hopkins,[3] F. Oehler,[2] S. Sivaraya,[3] R. A. Oliver,[2] C. J. Humphreys,[2] D. W. E. Allsopp,[3] and R. W. Martin[1]
[1]*Department of Physics, SUPA, University of Strathclyde, Glasgow G4 0NG, United Kingdom*
[2]*Department of Materials Science and Metallurgy, University of Cambridge, Cambridge CB3 0FS, United Kingdom*
[3]*Department of Electronic and Electrical Engineering, University of Bath, Bath BA2 7AY, United Kingdom*

(Received 7 January 2015; accepted 9 March 2015; published online 20 March 2015)

In this paper, we present a combined cathodoluminescence (CL) and electron beam induced current (EBIC) study of the optical and electrical properties of InGaN light emitting diodes grown using different active region growth methods. In one device, both the quantum wells and quantum barriers were deposited at their optimum temperatures (2 T), whereas in the other device, each barrier was grown in a two step process with the first few nanometers at a lower temperature (Q2T). It was found that in the Q2T sample, small micron scale domains of lower emission intensity correlate strongly to a lower EBIC signal, whereas in the 2 T sample which has a more uniform emission pattern and an anti-correlation exists between CL emission intensity and EBIC signal. [http://dx.doi.org/10.1063/1.4915628]

I. INTRODUCTION

The industry standard for high efficiency blue/white/green light emitting diodes (LEDs) involves the use of InGaN/GaN multi-quantum well (MQW)/quantum barrier (QB) active regions to increase carrier densities and radiative recombination efficiency. The high quality growth of these thin layers is of importance to both the optical and electrical characteristics of such devices. The optimum temperature for the growth of high quality GaN is around 1050 °C.[1] However, since indium nitride has a low dissociation temperature (550 °C),[2] GaN barriers have to be grown at lower temperatures to maintain high indium content in the wells. Aside from growing the barriers and wells at a single temperature, optimal for InGaN deposition (around 700–800 °C (Ref. 3))—which we define as the 1 T method—there are two methods used to balance indium desorption and barrier crystal quality. The first is the so called two-temperature (2 T)[3–5] approach, where the temperature is ramped up and down between around 900 °C for the barriers and 750 °C for the wells. This is expected to improve the crystal quality of the GaN, but results in an increased indium loss from the QW.[6] The second method, quasi two-temperature (Q2T),[2,6–9] is to grow the first few nanometers of the GaN barriers at the InGaN growth temperature before growing the remainder at the higher temperature, which serves to provide a protective cap on each quantum well. In this work, a fourth method was used where the temperature is ramped to around 800 °C after growth of the QWs before bringing it back down to grow the barriers at the low temperature. We refer to this as T-bounce (T-B),[10] and use it to investigate the importance of annealing the InGaN layer and of the barrier quality on the LED performance.

Cathodoluminescence (CL) imaging if often used to probe the luminescence characteristics of semiconductor optoelectronic devices, including laser diodes and LEDs. Panchromatic CL mapping provides information on the variation of total luminescence intensity across a sample, whereas hyperspectral imaging has proven to be of great use in mapping and correlating variations in the spectral emission parameters of epilayers,[11,12] MQW heterostructures,[13] and optoelectronic nanostructures.[14,15] However, CL is just one of several outcomes of the electron beam irradiation of a material. Measurement of the electron beam induced current (EBIC) complements CL because it adds extra information about the behaviour of generated charge carriers and probes the effect of electric fields in the device.[16–20]

Previous work on these samples[10] using transmission electron microscopy (TEM) has revealed that those grown without an annealing step (Q2T and 1 T) exhibit highly uniform quantum well thicknesses. By contrast, the devices where an anneal step is present (2 T, T-bounce) were shown to have significantly varying well thicknesses; in some the InGaN was not present at all, resulting in gaps in the quantum wells on a length scale of several tens of nanometers. These differences were found to affect the electroluminescence (EL) efficiency curves: non annealed samples had a lower peak efficiency by more than a factor of 2 compared to the 2 T and T-bounce devices, but this peak efficiency occurred at a much higher current density. The higher peak efficiency in the annealed, gappy quantum well devices was attributed to the localization of charge carriers in the pockets of InGaN QW and the prevention of diffusion to non-radiative sites.

II. METHOD

In this paper, we present a combined optoelectronic study of the InGaN/GaN LED structures described above. A set of four otherwise identical samples was grown with the 1 T, 2 T, Q2T, and T-B methods. The full growth details of

the samples are described by Oliver *et al.*[10] These were mapped by CL hyperspectral imaging using an electron beam acceleration voltage of 9 kV and beam current of 10 nA. A subsequent pair of devices grown with the Q2T and the 2 T methods was studied by EL mapping and simultaneous CL and EBIC imaging to investigate both the luminescence and the conductivity variations on a micron scale. We used an electron probe microanalyser (EPMA) to simultaneously perform the CL hyperspectral imaging and EBIC mapping of both devices with a spatial resolution of 1 μm. Electroluminescence measurements were carried out using the same EPMA scanning stage and optics. The electron beam was switched off and an 8 μm pinhole replaced the spectrograph entrance slit. The optical microscope in the EPMA has a magnification of approximately 3× which provides a spatial EL resolution of 3 μm.

The LEDs studied are *c*-plane III-N on sapphire grown by metal organic vapour phase epitaxy (MOVPE). All the structures studied consist of 2 μm *n*-type GaN, a 130 nm *p*-type GaN (inc p^+ contact layer), and a 5 period MQW active region. There was no electron blocking layer in any of the devices. The grown wafers were processed into $1 \times 1\,\text{mm}^2$ mesa etched, side contacted LEDs with an ~10 nm thick oxidized Ni/Au semi-transparent current spreading Ohmic contact on the *p*-layer. Non-alloyed Ti/Al contact stripes were formed on the *n*-layer (as an Ohmic contact) and over the Ni/Au in an interdigitated arrangement that minimizes current crowding. The LED wafers were mounted on TO-5 headers, where they were bonded with 5 μm Al wire. During EBIC measurements, a Keithley Instrument 2401 source/measure unit was used to hold the devices at a fixed voltage of 0 V and hence measure the short circuit current. At each point in the scan, a full CL spectrum was collected by an Andor CCD camera to build up a hyperspectral data-set. The CCD was also set to trigger the source/measure unit to take a measurement of the current with each spectral acquisition to simultaneously create an EBIC map of the same area. The data sets were analysed using customised software, and the spectra fitted to peak functions to create 2D maps of peak intensity and peak position. CL mapping was also performed on the LED as-grown wafers (pre-processing) but, since the LED contacts are required for current collection, corresponding EBIC could not be collected.

III. RESULTS

Under a forward current, Q2T and 2 T show markedly different patterns of emission. Figure 1 shows optical luminescence micrographs and EL integrated intensity maps taken of typical Q2T ((a) and (c)) and 2 T ((b) and (d)) grown LEDs under a 10 mA drive current. The emission from Q2T is dominated by bright spots and patches between 5 and 10 μm in size with an intensity variation of more than one decade between dark and bright. 2 T, in contrast, has a much more uniform appearance, with small variations, ~20%, and over a broader scale (~30–50 μm). Comparison with optical Nomarski micrographs suggests that the small intensity variations in the 2 T sample are related to its surface morphology.

In order to ascertain if the difference in emission was due to effects caused by processing of the LED wafers, CL

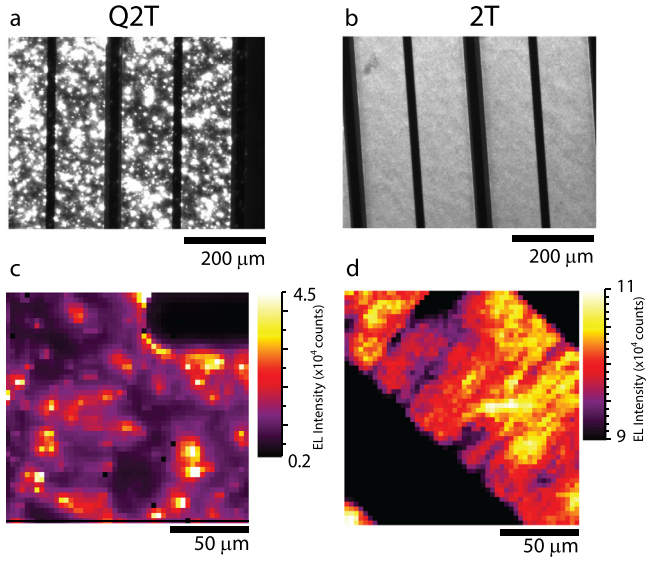

FIG. 1. Optical EL micrographs ((a) and (b)) and EL intensity maps ((c) and (d)) from a Q2T and 2 T LED under 10 mA drive current.

imaging was performed on 2 T and Q2T in both their processed (full device structure) and unprocessed (semiconductor layers only) forms. Figs. 2(a)–2(d) show $50 \times 50\,\mu\text{m}^2$ quantum well CL intensity maps from samples Q2T and 2 T in uncontacted LED and as-grown wafer form. In both forms, Q2T shows a high degree of non-uniformity in emission intensity: small regions, measuring 2–10 μm in size show a decrease in CL intensity by approximately a factor of 5 compared to the brightest areas. This is emphasized in the histograms and spectra in Figures 2(e) and 2(f). The Q2T histogram has a tail on the low intensity side which corresponds to the presence of the dark spots. Since the dark spots appear on both the processed and unprocessed wafer and have a very similar size, we can conclude that the cause is not due to the deposition of the current spreading layer or any other post-growth fabrication steps.

Figures 3(a), 3(b), 3(d), and 3(e) are a set of CL MQW intensity maps, taken under the same conditions, from the set of four *unprocessed* LED samples grown with the different active region temperature profiles. The intensity maps are plotted on the same relative scales and, as can be seen, the 1 T and Q2T samples have a similar spotty emission pattern to that of the Q2T LED from the first set, while T-B and 2 T are similarly comparable. This is demonstrated in Figures 3(c) and 3(f), which show the histograms and the coefficients of variation from the four maps, respectively. The coefficient of variation, COV, is defined by: $\text{COV} = \sigma/\bar{x}$, where σ is the standard deviation of the data set and $\bar{x}$ the mean. The distributions from the 1 T and Q2T in (c) clearly show an asymmetric tail on the low intensity side, which is directly attributable to the dark spots. The 2 T device has the highest average intensity and around twice that of the T-Bounce sample. In the previous study,[10] the EL efficiency from a large number of dies was studied, and it was found that T-bounce device had the highest internal quantum efficiency (IQE). A possible explanation for this could be due to the different way carriers are generated in CL compared to EL. In CL, carriers generated in and around the active region

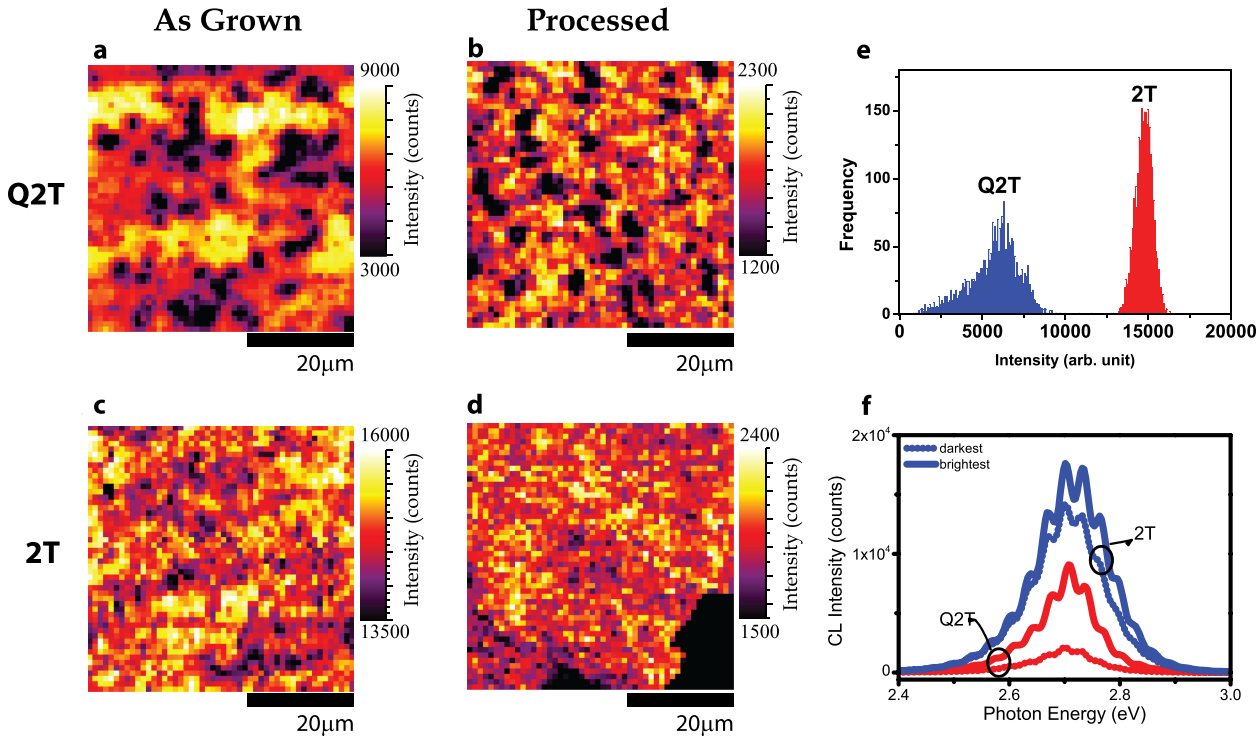

FIG. 2. MQW CL intensity maps of the Q2T ((a) and (b)) and 2 T ((c) and (d)) in unprocessed and LED form, respectively. Histograms (e) and CL spectra (f) taken from the "as grown" maps.

have, on average, a much higher energy than those which diffuse to the active region in EL.[20] In the latter case, the energy is only a few eV, around the energy of the bandgap, and can easily be captured by the quantum wells. For MQW luminescence, charge pairs generated by a high energy electron beam are required to lose significant energy before being captured by the QWs and so, in this time, there is an increased probability of non radiative recombination, mediated by barrier defects. Since the T-Bounce sample would be expected to have lower quality GaN barriers due to the lower growth temperature, it would result in more non-radiative recombination and lower CL than would be expected in the 2 T material. It is also worth noting that, since these samples are uncontacted, the electron beam will be inducing a

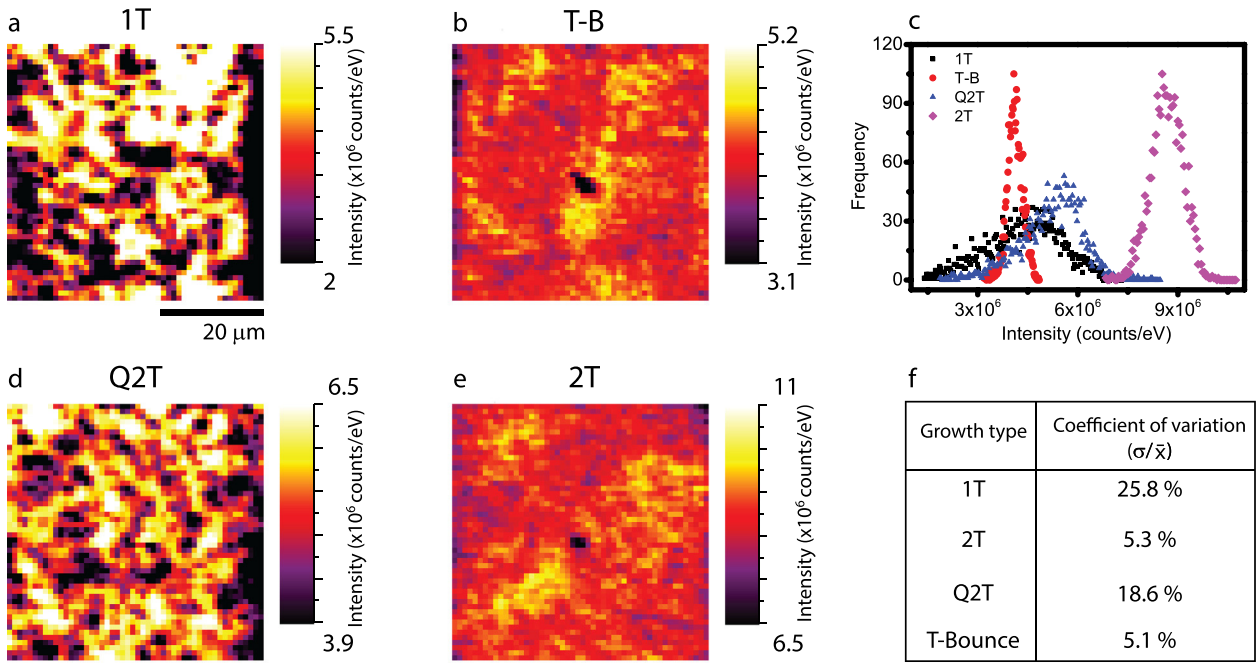

Growth type	Coefficient of variation ($\sigma/\bar{x}$)
1T	25.8 %
2T	5.3 %
Q2T	18.6 %
T-Bounce	5.1 %

FIG. 3. CL MQW intensity maps from the set of four as grown (uncontacted) LEDs; 1 T (a), T-B (b), Q2T (d), and 2 T (e). The maps are plotted on the same relative intensity scales. Histograms (c) and the calculated coefficients of variation (f) extracted from the four maps. The dark spots in the centre of (b) and (e) are due to electron beam damage during calibration.

forward voltage across the *p*/*n* junction due to excess carriers reducing the size of the depletion region[16,21] and the magnitude of this effect may vary from device to device.

These plots indicate that the four samples fall into two "families": those where there is no temperature ramp between quantum well and quantum barrier growth (1 T and Q2T) and those where there is a temperature ramp after barrier growth (2 T and T-bounce). The highest temperature to which the quantum wells are exposed is the same for all four devices, as it comes during the 950 °C anneal of the *p*-GaN performed to activate the acceptors. This suggests that the cause of the dark spots is related to whether or not the quantum wells are capped by a low temperature GaN layer *before* the ramp to high temperature. The previous study on these samples[10] also showed that the devices fall into these two families, with the capped having smooth wells and the uncapped having gappy wells.

Based on this first set of data, the EBIC/CL studies were performed on one type of LED from each "family," a 2 T and Q2T device which, based on the CL, are the brightest from each set. LEDs possessing a good *I*-*V* characteristic (i.e., with a low reverse leakage current) were chosen for EBIC measurements. The devices were biased at 0 V to measure the short circuit current. Figure 4 compares the CL data with the simultaneously collected EBIC signal for the Q2T and 2 T grown LEDs. (a)–(c) shows the fitted CL intensity and peak position, and EBIC maps of 2 T, while (d)–(f) are the equivalent maps for Q2T.

In the 2 T sample, an anti-correlation exists between the CL intensity and EBIC signal. Areas higher in luminescence intensity contribute less current to the external circuit when excited by the electron beam. There is also an anti-correlation between the intensity and fitted peak position, in that areas of lower intensity are also slightly blue-shifted by around 10 meV. These correlations are shown in the plot in Figures 5(a) and 5(b).

These relationships are consistent with competition between carrier escape from the active region and any form of recombination within the region. The scale of the variations indicate that these are the same as the broad variations seen in the EL in Figure 1 and those in the Nomarski images of the template referred earlier. A local decrease in the thickness of the quantum wells would cause a blue shift in the emission peak due to increase quantum confinement and an increase in the probability of carriers tunnelling out of the wells,[16,20] increasing the EBIC signal, and lowering the CL signal. The blueshift could also be caused by a local decrease in the InN content of the wells, and this would also be consistent with the increased EBIC and decreased CL because the reduction in band offset would enhance the probability of thermionic escape from the QWs or reduce capture probability.

The CL and EBIC maps and their correlations are quite different in the Q2T grown device. The most obvious feature from the EBIC map (Fig. 4(f)) is the presence of dark spots which coincide precisely with the dark features in the CL intensity map. These areas exhibit a lower radiative recombination rate that is not accounted for by an increase in carrier escape from the depletion region; in fact, the carrier escape is significantly lower also. This indicates unambiguously an increase in the non-radiative recombination rate. The correlation plot in Figure 5(b) demonstrates that the relationship between the CL intensity and EBIC is not as simple as in the 2 T material. Two sections of the plot exist; a positive correlation, which corresponds to the areas encompassing the

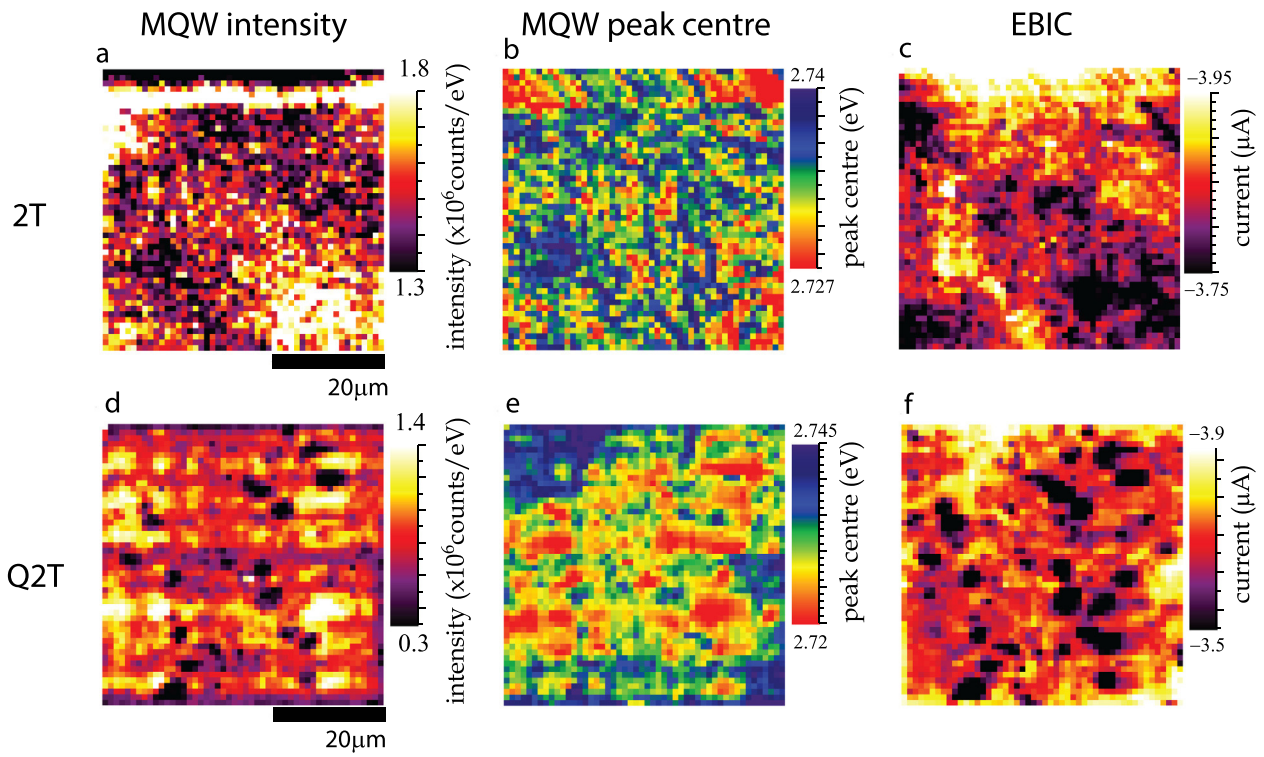

FIG. 4. CL intensity, CL peak position, and EBIC maps for the 2 T ((a)–(c)) and Q2T ((d)–(f)) devices.

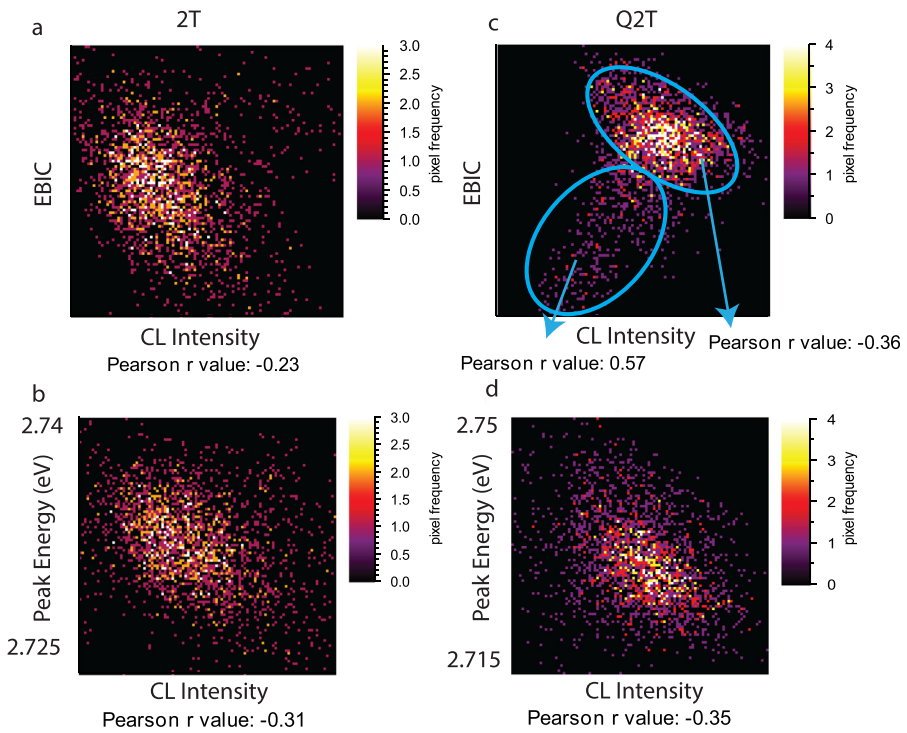

FIG. 5. Statistical correlation plots between CL MQW intensity and EBIC/CL peak centre for the 2 T ((a) and (b)) and the Q2T ((c) and (d)) LEDs. The Pearson *r* value is a measure of the strength of the correlation; a value of 1 denotes a perfect linear correlation: −1 denotes a perfect anti-correlation.

dark spots, and an anti-correlation, which at higher intensities has a Pearson *r* value very similar to that of the 2 T device. The relationship between the intensity and peak position is also similar to that of the 2 T material, in which the brighter areas are redshifted. This indicates that outside the dark spots the material is similar to that found in the 2 T device.

In order to determine what effect the dark areas have on the emission efficiency of the LEDs, we used EL mapping to spatially resolve the efficiency curves. Figures 6(a)–6(c) show EL maps at 10 mA, 100 mA, and 500 mA from a different area of the Q2T LED, where both the dark and bright spots can be resolved. At 10 mA, the emission is dominated by many small bright spots, around 3–10 μm in size (similar to Fig. 1(c)). As the current increases, the contrast from the bright spots drops and some of the dark spots become more apparent; at 500 mA, the luminescence is significantly more uniform, the COV having dropped from around 50% to 20%. Using these maps, we are able to spatially resolve the luminescence efficiency across the region and Figure 6(d) plots

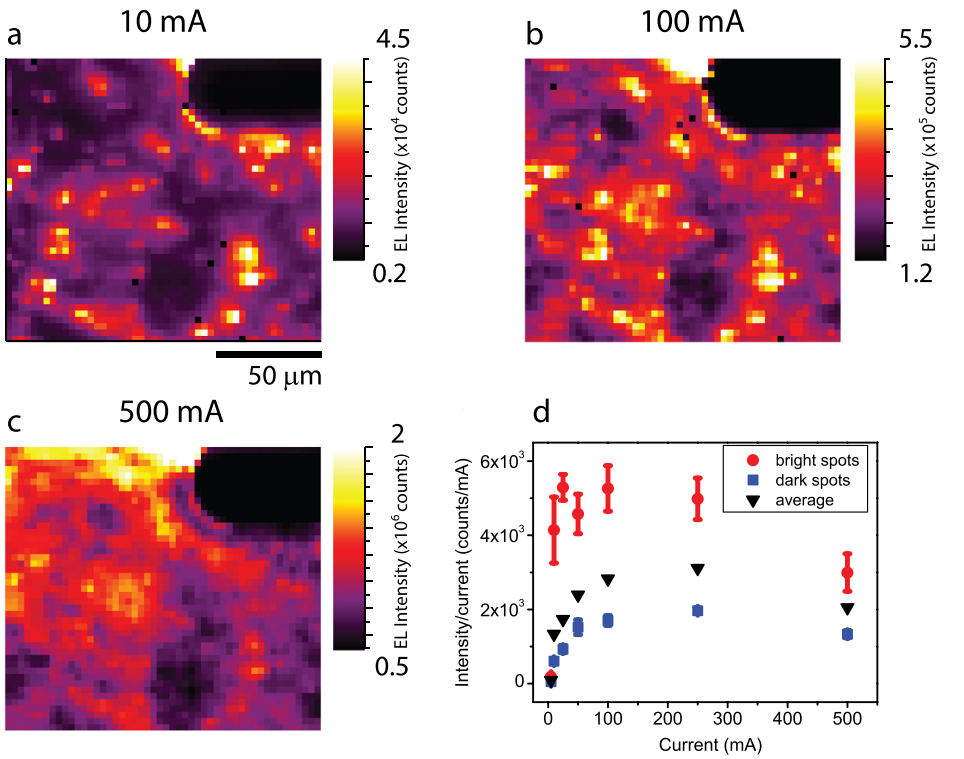

FIG. 6. EL intensity maps, from the Q2T LED, at 10 mA (a), 100 mA (b), and 500 mA (c). A pulsed current source with a 4% duty cycle was used to minimize heating effects. The plots in (d) are relative efficiency curves taken from several dark spots and bright regions.

L-I curves (intensity/current vs. current) for the average of several bright spots, dark spots, and the overall map average for several different currents. In the bright areas, efficiency droop occurs at or just below 100 mA, but in the dark areas, the onset of droop does not appear until several hundred milliamperes, a further indication that non-radiative recombination is more prevalent in the latter. More remarkable is the fact that the curve for the average intensity is almost identical to that of the dark spots. This would strongly suggest that the overall efficiency curve shape observed for the Q2T (and likely 1 T) devices is dominated by the dark spots, and that the areas outside the dark spots are more similar to the 2 T and T-B devices.

The low temperature capping of the quantum wells before the temperature ramp was done to prevent the break up of the InGaN on a nanoscale, but it has the unexpected effect of producing the observed dark spots on a micron scale. Potential causes were suggested (active region point defect clustering) and others ruled out (threading dislocation) in our previous work,[16] but the fact that they do not appear in the gappy QW devices indicates that the capping may, in fact, be preventing an important annealing step, which in the gappy QW devices anneals out these defects.

IV. CONCLUSION

In conclusion, we have demonstrated that the use of a simultaneous combination of cathodoluminescence hyperspectral imaging and electron beam induced current mapping to study the variations in luminescence and conductivity of InGaN/GaN LEDs grown with different barrier temperature profiles. Those devices where the quantum wells are uncapped prior to being exposed to a high temperature (2 T and T-B) were found to have uniform luminescence intensity and an anti-correlation between CL and EBIC, on a micron scale, due to competition between carrier recombination and escape from the active region. Where the devices are grown with a protective GaN low temperature cap (Q2T and 1 T), the luminescence in both CL and EL is dominated by dark spots 2–10 μm in size despite of having uniform quantum well thicknesses on a nanoscale. These dark spots are found to have a lower EBIC signal also indicating regions of non-radiative recombination and possible carrier trapping. The EL efficiency curves from the non-uniform samples vary across the sample, with the bright regions being more similar to the high temperature cap devices and the dark spots are found to have lower droop and appear to dominate the overall LED efficiency curve. We believe that the 2 T growth method represents the best manner, in which to grow LED active regions, primarily because the high temperature ramp upon the quantum wells effectively anneals out defects in the InGaN.

ACKNOWLEDGMENTS

This work was supported by the UK Engineering and Physical Sciences Research Council (EPSRC) (EP/I012591/1) Lighting the Future. The data associated with this research is available at: http://tinyurl.com/nomu5jr. Thanks go to Institute of Photonics (Strathclyde) for use of a wire bonder and Dr. Jochen Bruckbauer for helpful discussions.

[1]H. Amano, I. Akasaki, K. Hiramatsu, N. Koide, and N. Sawaki, Thin Solid Films **163**, 415 (1988).
[2]S. Pendlebury, P. Parbrook, D. Mowbray, D. Wood, and K. Lee, J. Cryst. Growth **307**, 363 (2007).
[3]S. Kret, F. Ivaldi, K. Sobczak, R. Czernecki, and M. Leszczyński, Phys. Status Solidi A **207**, 1101 (2010).
[4]E. Thrush, M. Kappers, P. Dawson, D. Graham, J. Barnard, M. Vickers, L. Considine, J. Mullins, and C. Humphreys, Phys. Status Solidi A **192**, 354 (2002).
[5]D. M. Graham, P. Dawson, M. J. Godfrey, M. J. Kappers, P. M. F. J. Costa, M. E. Vickers, R. Datta, C. J. Humphreys, and E. J. Thrush, Phys. Status Solidi C **3**, 1970 (2006).
[6]J.-W. Ju, H.-S. Kim, L.-W. Jang, J. H. Baek, D.-C. Shin, and I.-H. Lee, Nanotechnology **18**, 295402 (2007).
[7]P. M. F. J. Costa, R. Datta, M. J. Kappers, M. E. Vickers, C. J. Humphreys, D. M. Graham, P. Dawson, M. J. Godfrey, E. J. Thrush, and J. T. Mullins, Phys. Status Solidi A **203**, 1729 (2006).
[8]T. Zhu, H. A. El-Ella, B. Reid, M. J. Holmes, R. A. Taylor, M. J. Kappers, and R. A. Oliver, J. Cryst. Growth **338**, 262 (2012).
[9]S. J. Leem, Y. C. Shin, E. H. Kim, C. M. Kim, B. G. Lee, Y. Moon, I. H. Lee, and T. G. Kim, Semicond. Sci. Technol. **23**, 125039 (2008).
[10]R. A. Oliver, F. C.-P. Massabuau, M. J. Kappers, W. A. Phillips, E. J. Thrush, C. C. Tartan, W. E. Blenkhorn, T. J. Badcock, P. Dawson, M. A. Hopkins, D. W. E. Allsopp, and C. J. Humphreys, Appl. Phys. Lett. **103**, 141114 (2013).
[11]J. Christen, M. Grundmann, and D. Bimberg, J. Vac. Sci. Technol., B **9**, 2358 (1991).
[12]M. Avella, E. de la Puente, J. Jimenez, A. Castaldini, A. Cavallini, and L. Polenta, J. Cryst. Growth **210**, 220 (2000).
[13]J. Bruckbauer, P. R. Edwards, T. Wang, and R. W. Martin, Appl. Phys. Lett. **98**, 141908 (2011).
[14]P. R. Edwards, D. Sleith, A. W. Wark, and R. W. Martin, J. Phys. Chem. C **115**, 14031 (2011).
[15]K. J. Lethy, P. R. Edwards, C. Liu, W. N. Wang, and R. W. Martin, J. Appl. Phys. **112**, 023507 (2012).
[16]M. J. Wallace, P. R. Edwards, M. J. Kappers, M. A. Hopkins, F. Oehler, S. Sivaraya, D. W. E. Allsopp, R. A. Oliver, C. J. Humphreys, and R. W. Martin, J. Appl. Phys. **116**, 033105 (2014).
[17]E. Yakimov, S. Borisov, and S. Zaitsev, Semiconductors **41**, 411 (2007).
[18]E. Yakimov, P. Vergeles, A. Govorkov, A. Polyakov, N. Smirnov, I.-H. Lee, C. R. Lee, and S. Pearton, Superlattices Microstruct. **45**, 308 (2009).
[19]E. Yakimov, J. Surf. Invest. **6**, 887 (2012).
[20]U. Jahn, S. Dhar, M. Ramsteiner, and K. Fujiwara, Phys. Rev. B **69**, 115323 (2004).
[21]H. Masui, J. Sonoda, N. Pfaff, I. Koslow, S. Nakamura, and S. P. DenBaars, J. Phys. D: Appl. Phys. **41**, 165105 (2008).